Electronic Supplementary Material (ESI) for Sustainable Energy & Fuels.

Supporting Information

Evolution of "adsorption-insertion" K^+ storage behaviors in flower-like carbons with tunable heteroatom doping and graphitic structure

Wenrui Wei,‡ Haoran Lv,‡ Xuehui Wang,‡ Wenzhe Zhang, Zining Sun, Jing Shi, Minghua Huang, Shuai Liu, Zhicheng Shi, and Huanlei Wang*

School of Materials Science and Engineering, Ocean University of China, Qingdao, Shandong 266100, China

‡These authors contributed equally to this work.

*Corresponding author e-mail address: huanleiwang@gmail.com (Prof. H. Wang)

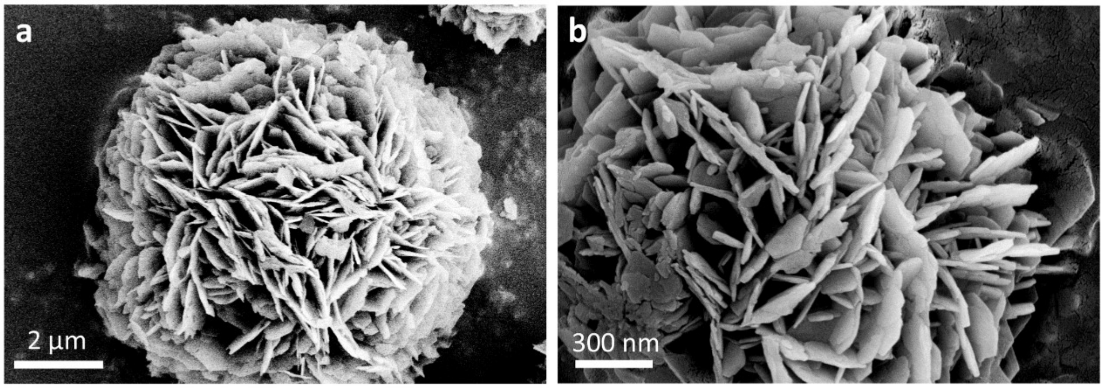

Fig. S1 Representative SEM images of BMS.

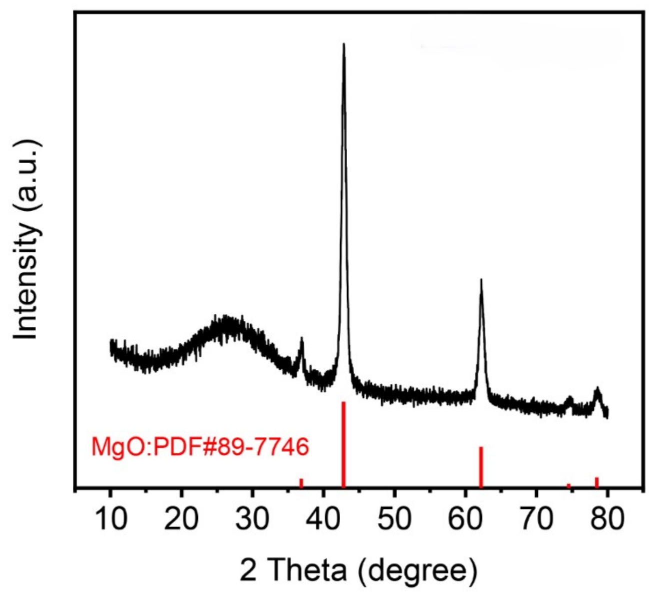

Fig. S2 XRD pattern of N,S-CNS without acid washing.

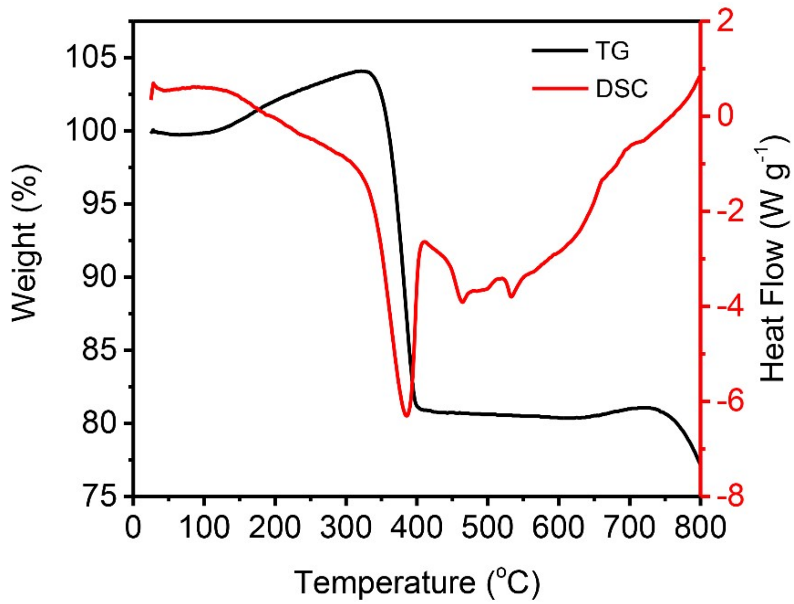

Fig. S3 TG-DSC curves of the BMS template.

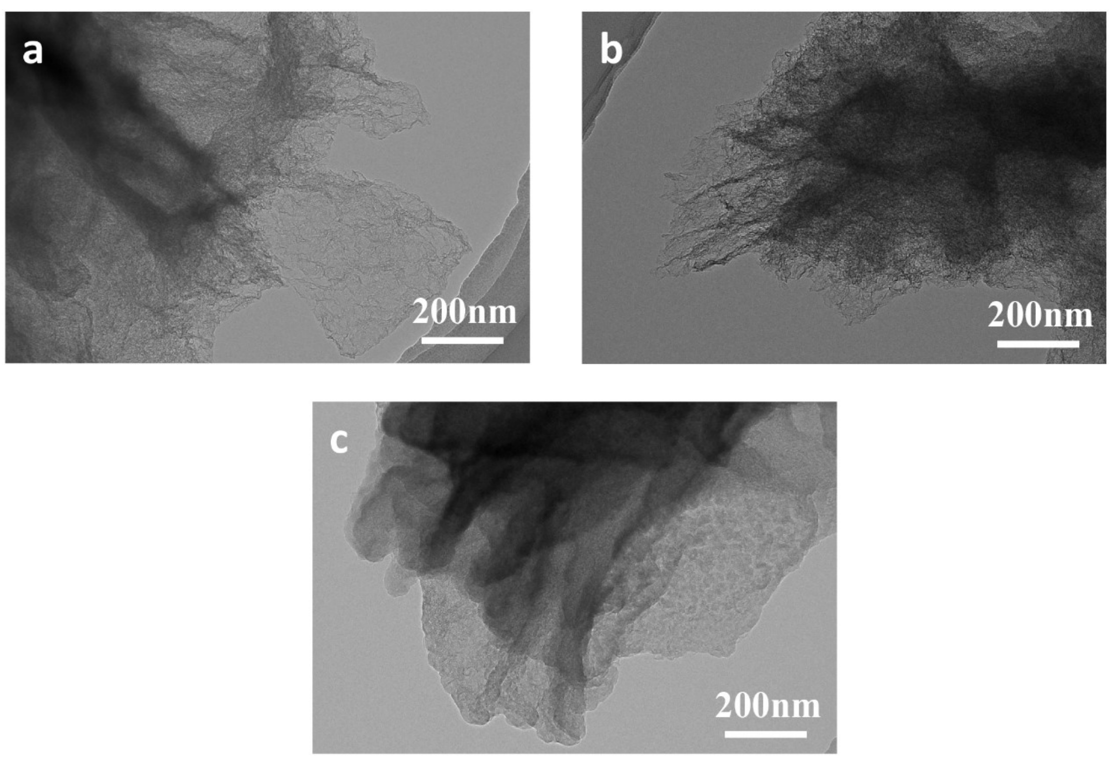

Fig. S4 Representative TEM images of (a) N,S-CNS, (b) N,S-CNS-900 and (c) N,S-CNS-1200.

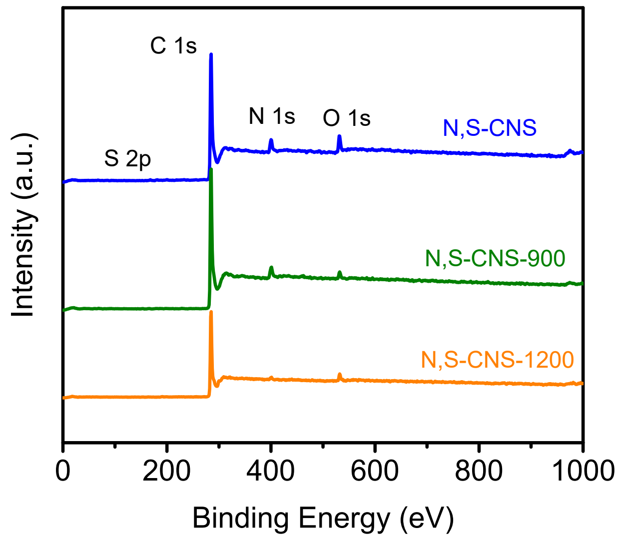

Fig. S5 The survey spectra of N,S-CNS, N,S-CNS-900 and N,S-CNS-1200.

Table S1. Textural properties and surface chemistry of N,S-CNSs.

Sample	Textural Properties				Surface Chemistry (XPS)				
	S_{BET}	V_{total}	Pore Volume (%)		C	O	S	N	$I_G/(I_G+I_D)$
	$m^2\ g^{-1}$	$cm^3\ g^{-1}$	$V_{<2nm}$	$V_{>2nm}$	at%	at%	at%	at%	
N,S-CNS	1263	0.95	30.8	69.2	88.50	5.10	0.27	6.13	0.356
N,S-CNS-900	1287	1.09	26.0	74.0	92.30	2.11	0.15	5.44	0.376
N,S-CNS-1200	1415	1.12	28.8	71.2	94.33	3.42	0.13	2.12	0.386

Table S2. Carbon bonding analysis of N,S-CNSs samples.

Binding Energy (eV)	Carbon Bonding	Concentration (%/at %)		
		N,S-CNS	N,S-CNS-900	N,S-CNS-1200
284.4	C=C	36.2/32.1	41.4/38.2	46.2/43.6
285.1	C-C	25.4/22.4	21.7/20.0	19.9/18.8
285.9	C-N	11.3/10.0	10.1/9.3	7.6/7.2
286.3	C-S	1.9/1.7	1.5/1.4	1.2/1.1
286.8	C-O	9.2/8.2	7.5/6.9	6.6/6.2
287.9	C=O	6.3/5.6	5.0/4.6	4.5/4.2
289.1	O-C=O	6.5/5.7	5.8/5.4	5.5/5.2
290.6	π-π	3.2/2.8	7.0/6.5	8.5/8.0
$sp^2/(sp^2+sp^3)$		58.9	65.6	69.9

Table S3. Nitrogen and Sulfur bonding analysis of N,S-CNSs samples.

	N [%]				S[%]		
	N-6	N-5	N-Q	N-O_x	S $2p_{3/2}$	S $2p_{1/2}$	C-SOx-C
N,S-CNS	27.8	52.1	14.6	5.5	12.3	6.1	81.6
N,S-CNS-900	29.7	46.5	16.3	7.5	44.1	21.9	34.0
N,S-CNS-1200	35.0	26.1	29.8	9.1	48.4	24.2	27.4

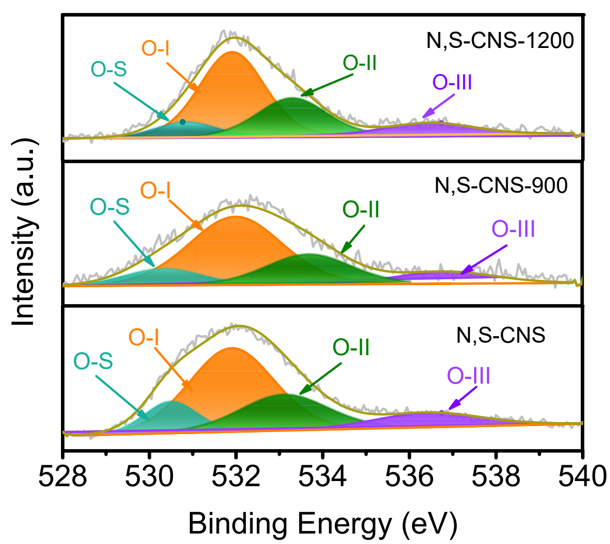

Fig. S6 High-resolution XPS spectra of O 1s for N,S-CNS, N,S-CNS-900, N,S-CNS-1200 and their corresponding fitting curves.

Table S4. ICE-Surface area detail data of N,S-CNS-1200 and other reported carbon anodes for PIBs.

Sample	Surface area (m^2 g^{-1})	ICE (%)	
N,S-CNS-1200	**1415**	**44.9**	**This work**
N-CNS[1]	674	20	Ref.1
rGO-aerogel[2]	219	26	Ref.2
NOHPHC[3]	1030	25	Ref.3
NCNF-650[4]	96	49	Ref.4
SNHC[5]	110	35	Ref.5
OFPCN[6]	1544	27	Ref.6
KC[7]	912	46	Ref.7
NPC[8]	341	43	Ref.8
ENPCS-500[9]	616	50	Ref.9
FFGF[10]	874	41	Ref.10
NPC[11]	316	30	Ref.11
S/N-CNFAS[12]	402	52	Ref.12
NBCNTs-1[13]	150	23	Ref.13
HENC[14]	110	46	Ref.14
S-MPC-700[15]	247	41	Ref.15
NSC[16]	436	50	Ref.16

BN-PC[17]	644	28	Ref.17
NCPs-600[18]	501	24	Ref.18

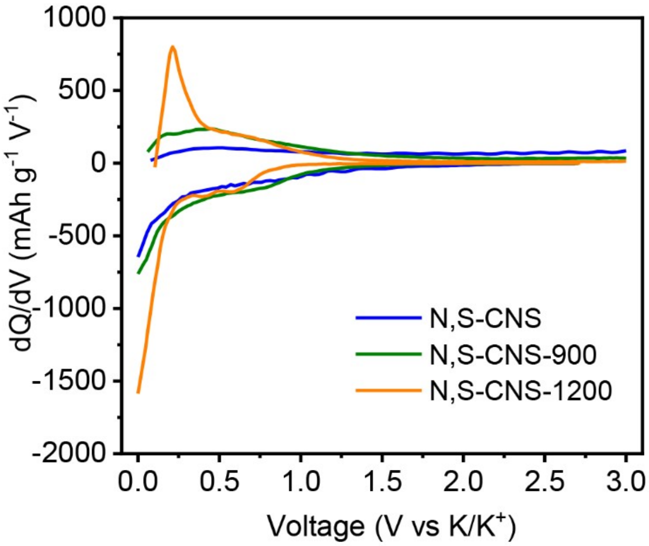

Fig. S7 Differential capacity vs. voltage for N,S-CNS, N,S-CNS-900 and N,S-CNS-1200 during the fifth cycle at the current of 0.05 A g^{-1}.

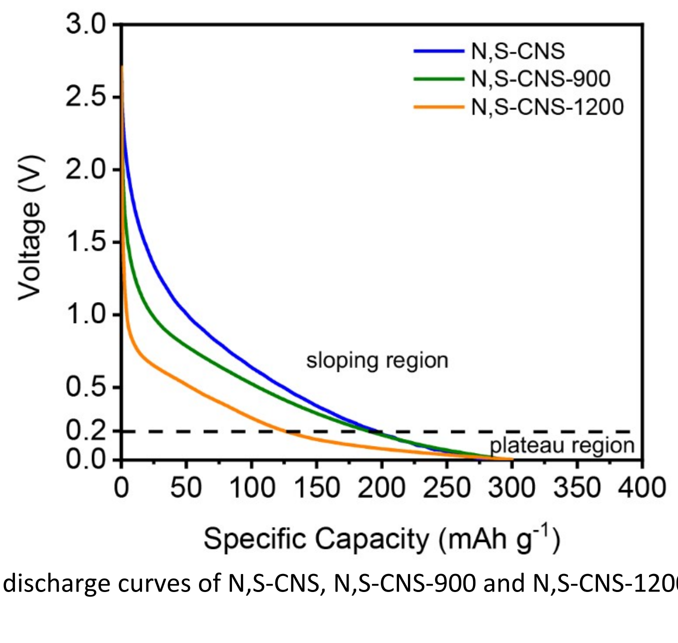

Fig. S8 Galvanostatic discharge curves of N,S-CNS, N,S-CNS-900 and N,S-CNS-1200 at the fifth cycle.

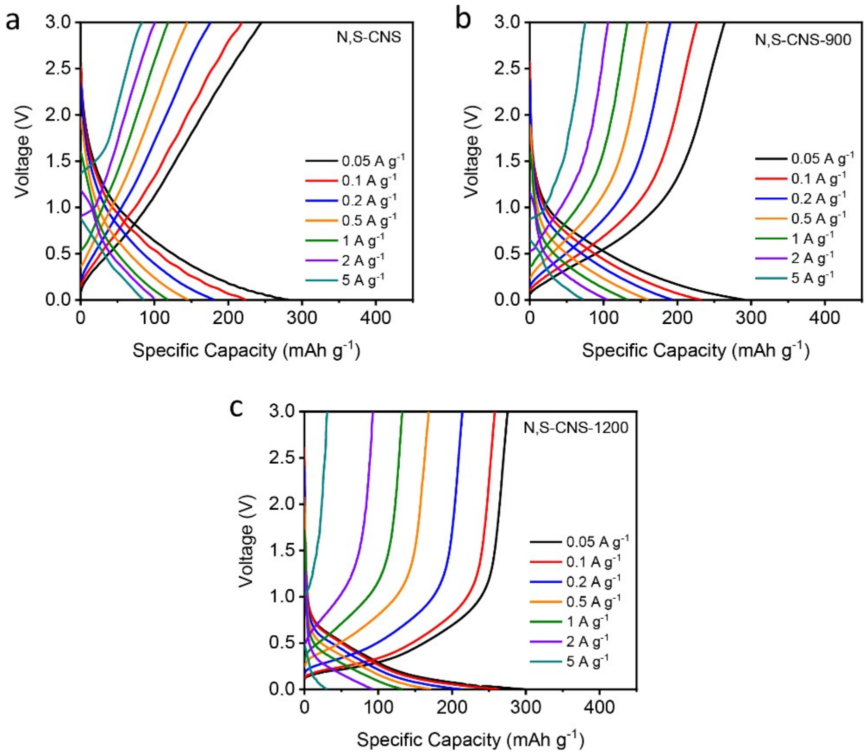

Fig. S9 Charge/discharge profiles of (a) N,S-CNS, (b) N,S-CNS-900 and (c) N,S-CNS-1200 at different current densities.

Table S5. The capacity contributions from sloping and plateau regions at various current densities.

	N,S-CNS		N,S-CNS-900		N,S-CNS-1200	
Current density (A g^{-1})	Capacity (mAh g^{-1})/ Capacity contribution (%)		Capacity (mAh g^{-1})/ Capacity contribution (%)		Capacity (mAh g^{-1})/ Capacity contribution (%)	
	Sloping	Plateau	Sloping	Plateau	Sloping	Plateau
0.05	195.1/69.2	87.0/30.8	189.1/63.7	107.6/36.3	125.7/42.1	172.6/57.9
0.1	164.6/73.5	59.4/26.5	157.1/67.6	75.2/32.4	118.1/44.5	147.2/55.5
0.2	131.0/72.3	50.2/27.7	132.5/68.3	61.6/31.7	103.7/47.9	112.8/52.1
0.5	105.3/72.2	40.6/27.8	106.6/66.5	53.8/33.5	87.7/52.4	79.8/47.6
1	85.4/72.1	33.1/27.9	83.4/62.6	49.8/37.4	69.6/52.3	63.5/47.7
2	75.0/75.4	24.5/24.6	61.6/58.2	44.3/41.8	40.5/43.5	52.7/56.5
5	60.8/70.9	25.0/29.1	36.2/50.0	36.3/50.0	8.3/27.2	22.2/72.8

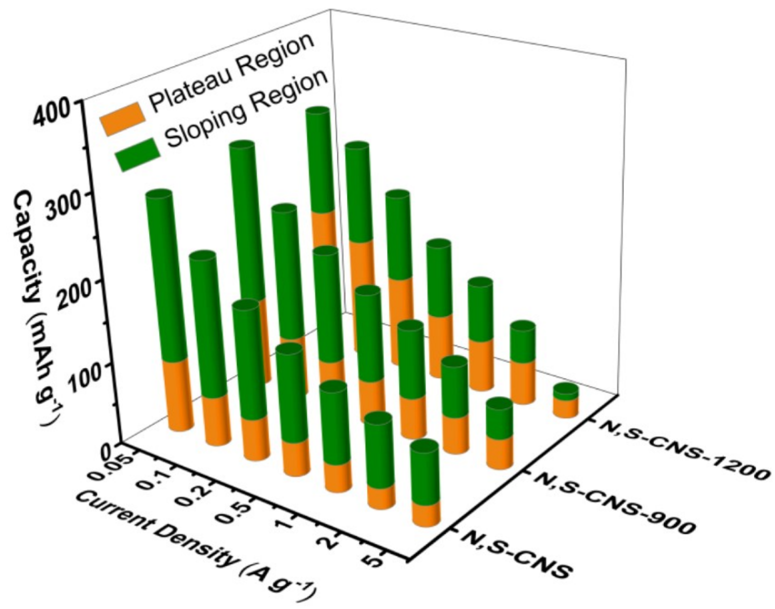

Fig. S10 The capacities from the sloping and plateau regions as a function of the current density.

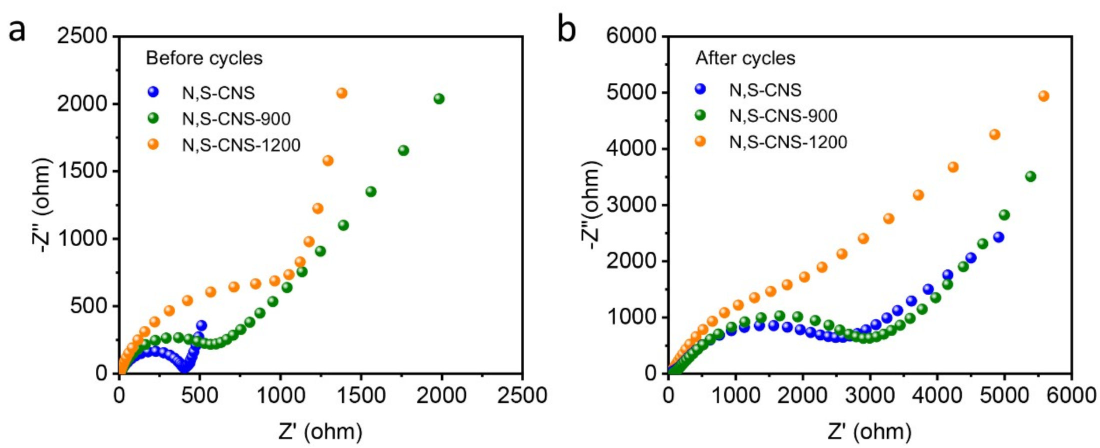

Fig. S11 Nyquist plots of N,S-CNS samples recorded at (a) before cycles and (b)after cycles.

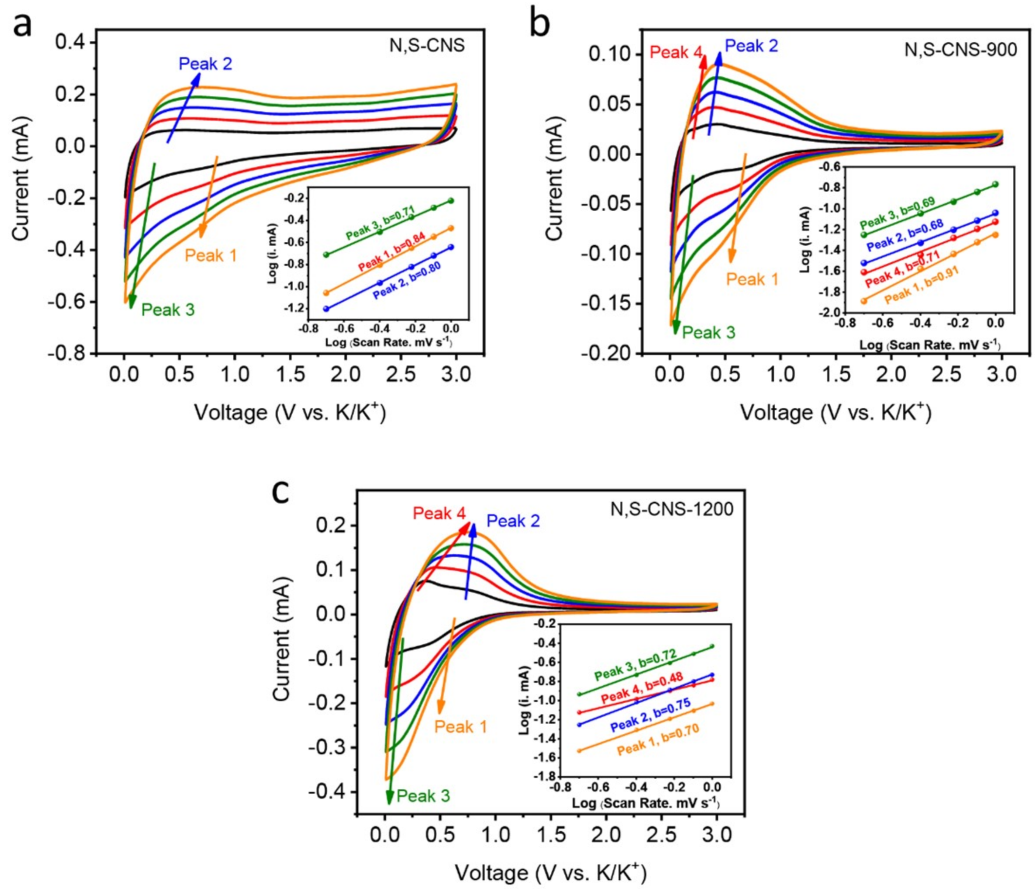

Fig. S12 CV profiles of (a) N,S-CNS, (b) N,S-CNS-900 and (c) N,S-CNS-1200 at different scan rates between 0.2 and 1.0 mV s^{-1} (Inset is b-value analysis using the relationship between peak current and scan rate).

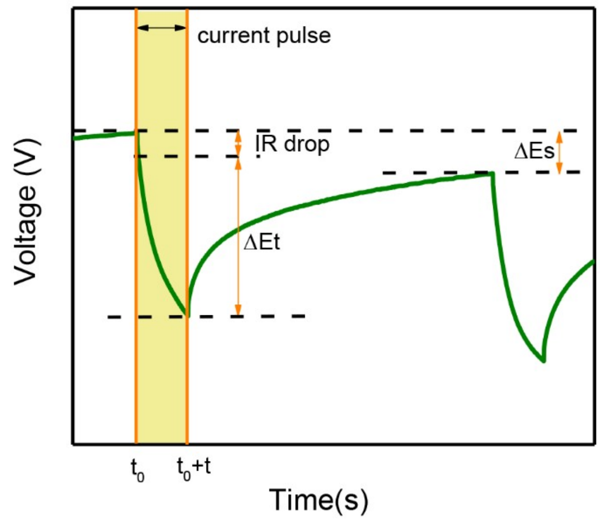

Fig. S13 The schematic illustration for the GITT calculation method.

The first cycle is tested by galvanostatic charge-discharge curves with a current density of 0.05 A g^{-1}, and the second cycle is examined by GITT. The test procedure involves the application of a galvanostatic pulse of 30 mA g^{-1} for 30 min, followed by a 3 h relaxation process. The ion diffusion (D_k) can be quantified as follow:[19, 20]

$$D_k = \frac{4}{\pi\tau}\left(\frac{m_B V_M}{M_B S}\right)^2\left(\frac{\Delta E_S}{\Delta E_\tau}\right)^2 \quad (4)$$

where the current pulse time is expressed as τ, V_M and m_B are the molar volume and the mass of the active material; the molar mass of carbon is M_B, S is the geometric contact area of the electrode; and ΔE_S and ΔE_τ are the potential changes during the integrated pulse-relaxation process.

Notes and references

1 L. Liu, Y. Chen, Y. Xie, P. Tao, Q. Li and C. Yan, *Adv. Funct. Mater.*, 2018, **28**, 1801989.
2 L. Liu, Z. Lin, J.-Y. Chane-Ching, H. Shao, P.-L. Taberna and P. Simon, *Energy Storage Mater.*, 2019, **19**, 306-313.
3 J. Yang, Z. Ju, Y. Jiang, Z. Xing, B. Xi, J. Feng and S. Xiong, *Adv. Mater.*, 2018, **30**, 1700104.
4 Y. Xu, C. Zhang, M. Zhou, Q. Fu, C. Zhao, M. Wu and Y. Lei, *Nat. Commun*, 2018, **9**, 1720.
5 Y. Liu, H. Dai, L. Wu, W. Zhou, L. He, W. Wang, W. Yan, Q. Huang, L. Fu and Y. Wu, *Adv. Energy Mater.*, 2019, **9**, 1901379.
6 J. Lu, C. Wang, H. Yu, S. Gong, G. Xia, P. Jiang, P. Xu, K. Yang and Q. Chen, *Adv. Funct. Mater.*, 2019, **29**, 1906126.
7 D. Li, Q. Sun, Y. Zhang, X. Dai, F. Ji, K. Li, Q. Yuan, X. Liu and L. Ci, *Nano Res*, 2021, 2021, **21**, 3324.
8 D. Li, X. Ren, Q. Ai, Q. Sun, L. Zhu, Y. Liu, Z. Liang, R. Peng, P. Si, J. Lou, J. Feng and L. Ci, *Adv. Energy Mater.*, 2018, **8**, 1802386.
9 F. Xu, Y. Zhai, E. Zhang, Q. Liu, G. Jiang, X. Xu, Y. Qiu, X. Liu, H. Wang and S. Kaskel, *Angew. Chem. Int. Edit.*, 2020, **59**, 19460-19467.
10 Z. Ju, S. Zhang, Z. Xing, Q. Zhuang, Y. Qiang and Y. Qian, *ACS Appl. Mater. Interfaces*, 2016, **8**, 20682-20690.
11 X. Qi, K. Huang, X. Wu, W. Zhao, H. Wang, Q. Zhuang and Z. Ju, *Carbon*, 2018, **131**, 79-85.
12 C. Lv, W. Xu, H. Liu, L. Zhang, S. Chen, X. Yang, X. Xu and D. Yang, *Small*, 2019, **15**, 1900816.
13 Y. Liu, C. Yang, Q. Pan, Y. Li, G. Wang, X. Ou, F. Zheng, X. Xiong, M. Liu and Q. Zhang, *J. Mater. Chem. A*, 2018, **6**, 15162-15169.
14 Y. Zhao, Z. Sun, Y. Yi, C. Lu, M. Wang, Z. Xia, X. Lian, Z. Liu and J. Sun, *Nano Res*, 2021, **14**, 1413-1420.
15 Y. Zuo, P. Li, R. Zang, S. Wang, Z. Man, P. Li, S. Wang and W. Zhou, *ACS Appl. Energy Mater.*, 2021, **4**, 2282-2291.
16 Q. Liu, F. Han, J. Zhou, Y. Li, L. Chen, F. Zhang, D. Zhou, C. Ye, J. Yang, X. Wu and J. Liu, *ACS Appl. Mater. Interfaces*, 2020, **12**, 20838-20848.
17 W. Feng, N. Feng, W. Liu, Y. Cui, C. Chen, T. Dong, S. Liu, W. Deng, H. Wang and Y. Jin, *Adv. Energy Mater.*, 2021, **11**, 2003215.
18 S. Xu, L. Cai, P. Niu, Z. Li, L. Wei, G. Yao, C. Wang, F. Zheng and Q. Chen, *Carbon*, 2021, **178**, 256-264.
19 K. Tang, X. Yu, J. Sun, H. Li and X. Huang, *Electrochim. Acta*, 2011, **56**, 4869-4875.
20 D. Qiu, J. Guan, M. Li, C. Kang, J. Wei, Y. Li, Z. Xie, F. Wang and R. Yang, *Adv. Funct. Mater.*, 2019, **29**, 1903496.